inorganics

MDPI

Review

Vanadium Oxide-Based Cathode Materials for Aqueous Zinc-Ion Batteries: Energy Storage Mechanism and Design Strategy

Yu Qiu, Zhaoqian Yan, Zhihao Sun, Zihao Guo, Hongshou Liu, Benli Du, Shaoyao Tian, Peng Wang, Han Ding and Lei Qian *

Key Laboratory for Liquid-Solid Structural Evolution and Processing of Materials, (Ministry of Education), Shandong University, 17923 Jingshi Road, Jinan 250061, China
* Correspondence: qleric@sdu.edu.cn

Abstract: Aqueous zinc ion batteries (AZIBs) are an ideal choice for a new generation of large energy storage devices because of their high safety and low cost. Vanadium oxide-based materials have attracted great attention in the field of AZIB cathode materials due to their high theoretical capacity resulting from their rich oxidation states. However, the serious structural collapse and low intrinsic conductivity of vanadium oxide-based materials cause rapid capacity fading, which hinders their further applications in AZIB cathode materials. Here, the structural characteristics and energy storage mechanisms of vanadium oxide-based materials are reviewed, and the optimization strategies of vanadium oxide-based cathode materials are summarized, including substitutional doping, vacancy engineering, interlayer engineering, and structural composite. Finally, the future research and development direction of vanadium oxide-based AZIBs are prospected in terms of cathode, anode, electrolyte, non-electrode components, and recovery technology.

Keywords: aqueous zinc ion batteries; vanadium oxide−based cathode; energy storage mechanism; design strategy

check for updates

Citation: Qiu, Y.; Yan, Z.; Sun, Z.; Guo, Z.; Liu, H.; Du, B.; Tian, S.; Wang, P.; Ding, H.; Qian, L. Vanadium Oxide-Based Cathode Materials for Aqueous Zinc-Ion Batteries: Energy Storage Mechanism and Design Strategy. *Inorganics* **2023**, *11*, 118. https://doi.org/10.3390/inorganics11030118

Academic Editors: Duncan H. Gregory and Christian Julien

Received: 10 February 2023
Revised: 6 March 2023
Accepted: 10 March 2023
Published: 12 March 2023

Copyright: © 2023 by the authors. Licensee MDPI, Basel, Switzerland. This article is an open access article distributed under the terms and conditions of the Creative Commons Attribution (CC BY) license (https://creativecommons.org/licenses/by/4.0/).

1. Introduction

With the continuous advancement of the global carbon neutrality strategy, the share of renewable energy (wind and water resources, etc.) in global power production has gradually increased [1–3]. However, due to the intermittence and uncontrollability of wind and solar resources, the stability of the power-system will be destroyed when wind and solar resources are directly input into the power grid [2,4]. As a result, it is urgently necessary for an advanced energy storage device to coordinate the power transmission between these unstable energy sources and the power grid [5]. Lithium-ion batteries (LIBs) are excellent representatives of energy storage devices. However, LIBs also have safety problems caused by organic electrolytes and lithium dendrites, as well as high cost problems and harsh process conditions, which limit their larger-scale applications [6,7].

Aqueous batteries directly use an aqueous solution as an electrolyte, which fundamentally solves the safety problems caused by organic electrolytes. In addition, aqueous batteries have the advantages of excellent ion conductivity, low cost, and low toxicity [8–11]. Aqueous zinc ion batteries (AZIBs), which are one of the different types of aqueous batteries, are an ideal choice for the next generation of large-scale energy storage devices due to the high stability of zinc, high theoretical specific capacity, abundant reserves, and the inexpensive price of zinc [12–16]. However, the strong Coulomb interaction between divalent Zn^{2+} and the main framework of cathode materials prevents greater ion diffusion kinetics from being achieved, despite the ionic radius of Zn^{2+} (0.74 Å) being relatively moderate [17]. Even if the structural water molecules can effectively reduce the high charge density of Zn^{2+} to a certain extent

through the charge shielding effect, the large radius of hydrated Zn^{2+} undoubtedly puts forward higher requirements on the openness and stability of the main frame of cathode materials [17,18].

Among the reported cathode materials for AZIBs, the host materials that can achieve reversible deintercalation of Zn^{2+} are mainly concentrated in Prussian blue analogues, organic polymer materials, manganese-based compounds, and vanadium oxide-based materials [19]. However, the former three have serious problems during Zn^{2+} insertion/extraction, such as the unsatisfactory theoretical capacity of Prussian blue analogues, the dissolution of organic polymer materials in aqueous electrolytes, and the structural collapse of manganese-based compounds [19]. These defects limit their development as AZIB cathode materials. Owing to vanadium's multi-variable valence state and the V-O polyhedron layer's high level spacing, vanadium oxide-based materials exhibit high specific capacities, long cycle stability, and better ion diffusion kinetics when compared to other AZIB cathode materials (Table 1) [20]. Although vanadium oxide-based materials also have the problems of structural collapse and the dissolution of active substances, the collapse and dissolution of vanadium oxide-based materials are less than manganese-based compounds because of the steadier oxidation state and structure.

Table 1. Performance comparison of vanadium oxide-based cathode materials.

Cathode	Electrolyte	Specific Capacity (Current Density)	Cyclic Stability (Cycles, Current Density)	Ref.
V_2O_5	3M $Zn(CF_3SO_3)_2$	319 mAh g^{-1} (0.02 A g^{-1})	81% (2000, 2.0 A g^{-1})	[21]
V_2O_5	3M $Zn(CF_3SO_3)_2$	503.1 mAh g^{-1} (0.1 A g^{-1})	86% (700, 0.5 A g^{-1})	[22]
VO_2(B)	1M $ZnSO_4$	325.6 mAh g^{-1} (0.05 A g^{-1})	86% (5000, 3.0 A g^{-1})	[23]
VO_2(B)	1M $ZnSO_4$	353 mAh g^{-1} (1.0 A g^{-1})	75.5% (945, 3.0 A g^{-1})	[24]
VO_2(B)	3M $Zn(CF_3SO_3)_2$	274 mAh g^{-1} (0.1 A g^{-1})	79% (10,000, 10.0 A g^{-1})	[25]
VO_2(D)	3M $ZnSO_4$	408 mAh g^{-1} (0.1 A g^{-1})	58% (10,000, 10.0 A g^{-1})	[26]
V_2O_3	3M $Zn(CF_3SO_3)_2$	382.5 mAh g^{-1} (0.8 A g^{-1})	97.3% (800, 3.2 A g^{-1})	[27]
V_2O_3	2M $Zn(CF_3SO_3)_2$	625 mAh g^{-1} (0.1 A g^{-1})	100 % (10,000, 10.0 A g^{-1})	[28]
V_6O_{13}	3M $Zn(CF_3SO_3)_2$	360 mAh g^{-1} (0.2 A g^{-1})	92% (2000, 4.0 A g^{-1})	[29]

With the rapid development of vanadium oxide-based materials in AZIB cathode materials, it is necessary to summarize their latest progress. In this review, we analyze the vanadium oxide-based materials in detail from the aspects of structural characteristics, energy storage mechanisms, and design strategy. Firstly, we describe the structural characteristics of vanadium oxide-based materials and several typical energy storage mechanisms (Figure 1). Secondly, we describe the design strategy of typical vanadium oxide-based cathode materials. Finally, future research directions and prospects of AZIB cathode materials are prospected.

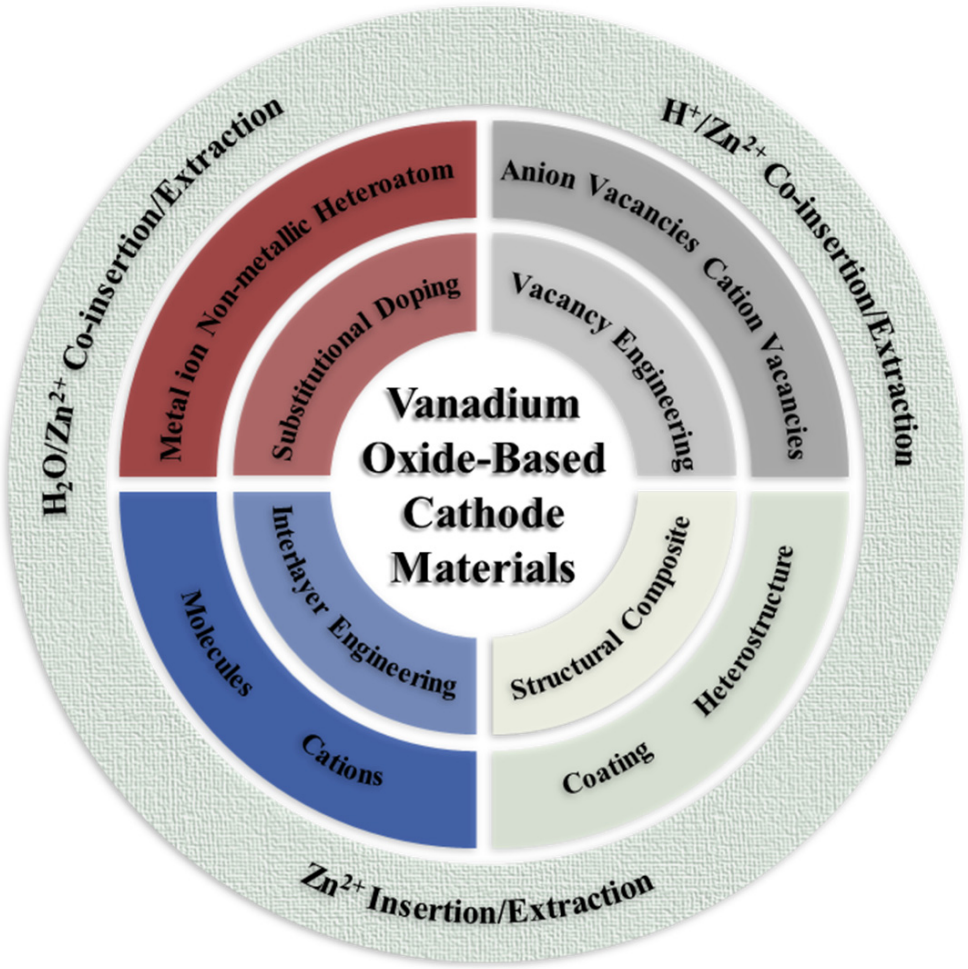

Figure 1. Overview of energy storage mechanisms and design strategy from vanadium oxide-based cathode materials for AZIBs.

2. Energy Storage Mechanisms of Vanadium Oxide-Based Cathodes

There are several different oxidation states for vanadium, including V^{5+}, V^{4+}, and V^{3+} [20]. Vanadium in different oxidation states can coordinate with oxygen to form various types of V-O polyhedrons, including VO_4 tetrahedron, VO_5 square pyramid, trigonal bipyramid, regular octahedron, and distorted octahedron (Figure 2a) [30]. The valence state of vanadium in VO_4 tetrahedron must be +5, while the valence states of VO_5 square pyramids and trigonal bipyramids are +5 or +4. For V-O octahedron (including a regular octahedron and distorted octahedron), the vanadium ions are usually V^{5+}, V^{4+}, or V^{3+}, and even lower valence V^{2+}. Different vanadium oxide-based materials are usually assembled by different types of V-O coordination polyhedrons. For example, V_2O_5 is a layered structure formed by the corner-sharing of VO_5 square pyramids [31], and VO_2(B) is a tunnel-like structure consisting of the edge-sharing of VO_6 octahedron. Therefore, in the electrochemical reaction process, the structure of the V-O framework varies significantly with the oxidation state of vanadium, thus forming vanadium oxide-based materials with different phases. This change is beneficial to inhibit the crystal structure degradation during the Zn^{2+} insertion/extraction process to maintain the stability of the structure, and also provides more redox reaction paths for the electrochemical reaction process [9].

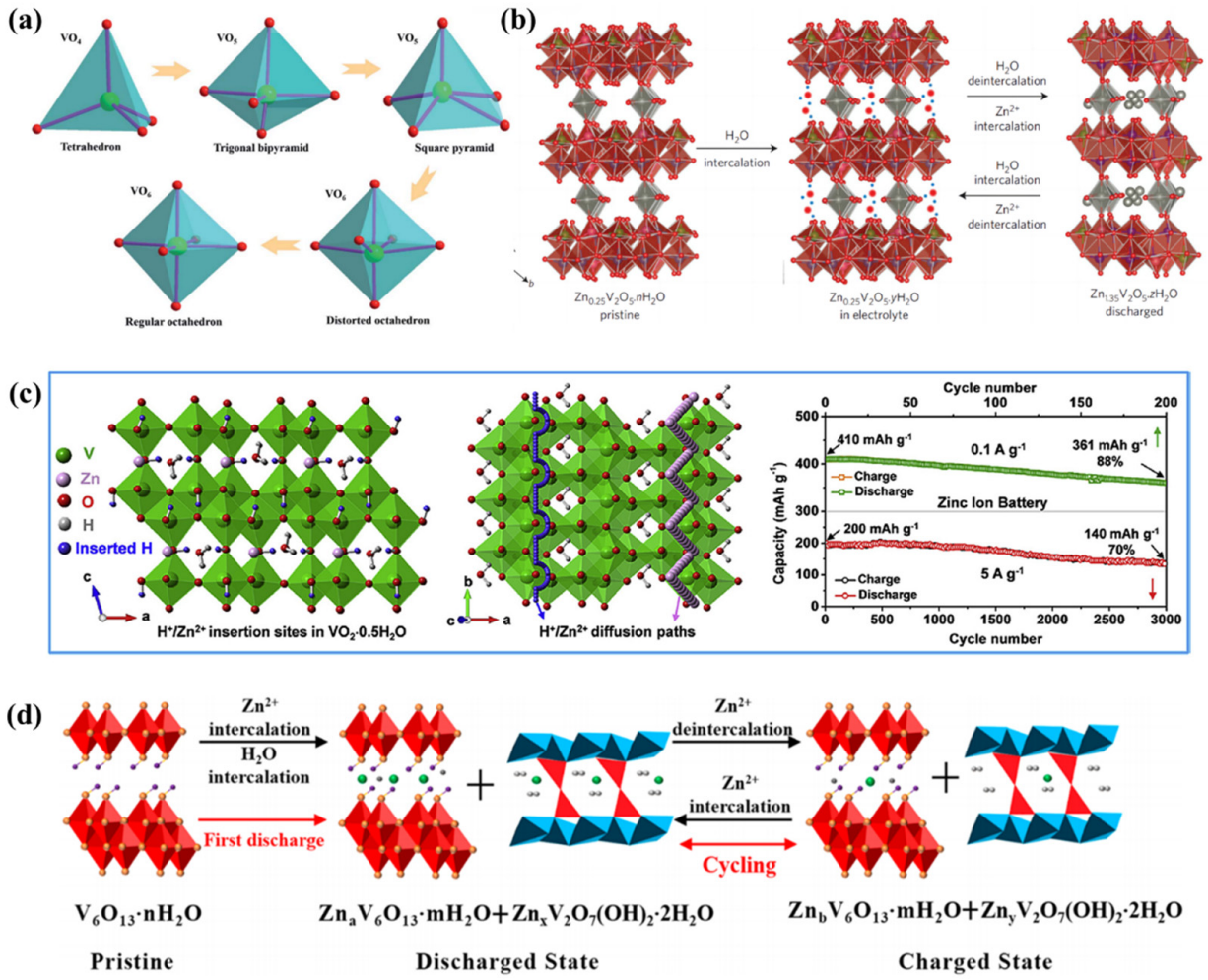

Figure 2. (**a**) Classification of V-O coordination polyhedron (Ref. [20]). (**b**) Structural changes of $Zn_{0.25}V_2O_5{\cdot}nH_2O$ during electrochemical reaction (Ref. [32]). (**c**) The insertion site (**left**) and migration pathway (**middle**) of Zn^{2+} and H^+ during charging and the long cycle performance (**right**) of $VO_2{\cdot}0.45H_2O$ (Ref. [33]). (**d**) A schematic diagram of reversible extraction/insertion of Zn^{2+} and water molecules in $V_6O_{13}{\cdot}nH_2O$ during initial charge/discharge and subsequent processes (Ref. [34]).

Due to the diversity of the compositions and structural frameworks of vanadium oxide-based materials, there are many energy storage mechanisms in aqueous zinc ion batteries: Zn^{2+} insertion/extraction, H^+/Zn^{2+} co-insertion/extraction, and H_2O/Zn^{2+} co-insertion/extraction mechanism.

2.1. Zn^{2+} Insertion/Extraction Mechanism

Vanadium oxide-based materials often have open structures (tunnel, layered, etc.), and their large voids contribute to the insertion of Zn^{2+}. Typical V_2O_5 shows a Zn^{2+} insertion/extraction mechanism. In the electrochemical reaction process, Zn^{2+} is embedded into the interlayer of V_2O_5 to form $Zn_xV_2O_5$ [35]. Metal ion-intercalated hydrated V_2O_5 ($M_xV_2O_5{\cdot}nH_2O$, M = metal) also adopts the Zn^{2+} insertion/extraction mechanism. For example, Kundu et al. synthesized $Zn_{0.25}V_2O_5{\cdot}nH_2O$ by introducing Zn^{2+} and H_2O as 'pillars' between the V_2O_5 layers (Figure 2b) [32]. During charge and discharge, $Zn_{0.25}V_2O_5{\cdot}nH_2O$ exhibited a reversible insertion/extraction process of Zn^{2+}:

$$\text{Anode: } 1.1Zn \leftrightarrow 1.1Zn^{2+} + 2.2e^-$$

$$\text{Cathode: } 1.1Zn^{2+} + 2.2e^- + Zn_{0.25}V_2O_5{\cdot}nH_2O \leftrightarrow Zn_{1.35}V_2O_5{\cdot}nH_2O$$

2.2. H^+/Zn^{2+} Co-Insertion/Extraction Mechanism

The electrolyte of AZIBs is mainly composed of inorganic zinc salt solutions such as $ZnSO_4$, $Zn(CF_3SO_3)_2$, and $ZnCl_2$, which are usually weakly acidic [36]. In these inorganic zinc salt solutions, in addition to Zn^{2+}, there are also a lot of H^+. This results in a synergistic insertion/extraction mechanism between Zn^{2+} and H^+ in some vanadium oxide-based cathode materials during charging/discharging. The lower charge valence and smaller volume of H^+ make it have higher diffusion kinetics, and the lattice distortion caused by the insertion/extraction process is much smaller than that of Zn^{2+}. Therefore, a long cycle life and an outstanding rate performance are more likely to be displayed by cathode materials with H^+/Zn^{2+} co-insertion/extraction mechanisms. Zhu et al. reported the reversible electrochemical reaction between $VO_2{\cdot}0.45H_2O$ cathode and zinc foil anode [33]. $VO_2{\cdot}0.45H_2O$ cathode material based on H^+/Zn^{2+} co-insertion/extraction mechanism enabled AZIBs to obtain long cycle stabilities at both low and high current densities (Figure 2c). The specific reaction mechanism is as follows:

$$\text{Anode: } Zn \leftrightarrow Zn^{2+} + 2e^-$$

$$\text{Cathode: } VO_2{\cdot}0.5H_2O + H^+ + e^- \leftrightarrow HVO_2{\cdot}0.5H_2O$$

$$H_2O \leftrightarrow OH^- + H^+$$

$$Zn^{2+} + 2OH^- \leftrightarrow Zn(OH)_2$$

2.3. H_2O/Zn^{2+} Co-Insertion/Extraction Mechanism

H_2O/Zn^{2+} co-insertion/extraction mechanisms are often observed in some vanadium oxide-based materials, such as V_2O_5 and V_6O_{13}. During the electrochemical reaction process, the solvated water can be used as a charge shielding medium, thereby weakening the Coulomb force between Zn^{2+} and the V-O polyhedral framework [18]. The presence of solvated water makes Zn^{2+} obtain faster ion diffusion kinetics in the insertion/extraction process, realizing the 'self-lubricating' effect of the ion transport. Lai et al. reported the Zn^{2+}/H_2O co-insertion/extraction mechanism in $V_6O_{13}{\cdot}nH_2O$ cathode materials (Figure 2d) [34]. During charging and discharging, H_2O was embedded in the $V_6O_{13}{\cdot}nH_2O$ cathode to form $Zn_aV_6O_{13}{\cdot}mH_2O$. The introduction of water molecules greatly reduced the effective charge of Zn^{2+}, thereby shielding the Coulomb force with the V_6O_{13} skeleton and significantly improving the ion diffusion kinetics of Zn^{2+}.

3. Design Strategies for Vanadium Oxide-Based Cathode

3.1. Substitutional Doping

Doping is a very effective modification strategy. It introduces metal ions or non-metallic heteroatoms into the structure of cathode materials by in situ or ex situ methods. Doping ions/atoms can adjust the electronic distribution of cathode materials to optimize the electrochemical performance [37].

Metal-ion doping is a very promising strategy to solve the problems of high solubility in aqueous electrolytes, poor intrinsic conductivity, and structural collapse during the charging/discharging of vanadium oxide-based cathode materials [38]. Metal-ion doping alleviates the dissolution of vanadium to a certain extent and inhibits the structural degradation of vanadium oxide-based materials. The doped materials have more abundant active sites, stable structures, and excellent conductivity. Liu et al. controllably synthesized Ni-doped V_6O_{13} ($Ni_xV_{6-x}O_{13}$) nanobelts by a one-step hydrothermal method and used them as cathodes in AZIBs (Figure 3a) [39]. The $Ni_xV_{6-x}O_{13}$ cathode material had an excellent conductivity, high interlayer spacing, and abundant reaction sites (Figure 3b,c). Finally, the $Ni_xV_{6-x}O_{13}$ cathode material achieved a high specific capacity and excellent cycle performance (Figure 3e). Li et al. reported Al-doped $V_{10}O_{24}{\cdot}12H_2O$ as a cathode material for AZIBs (Figure 3d) [40]. Al-doped $V_{10}O_{24}{\cdot}12H_2O$ had a longer cycle life and could provide a higher capacity (Figure 3e). Due to the different electron distributions and

radii between the metal ions, the introduction of different metal ions as dopants produces different charge structure changes and lattice distortions. This leads to the difference in cathode electrochemical performance (Table 2).

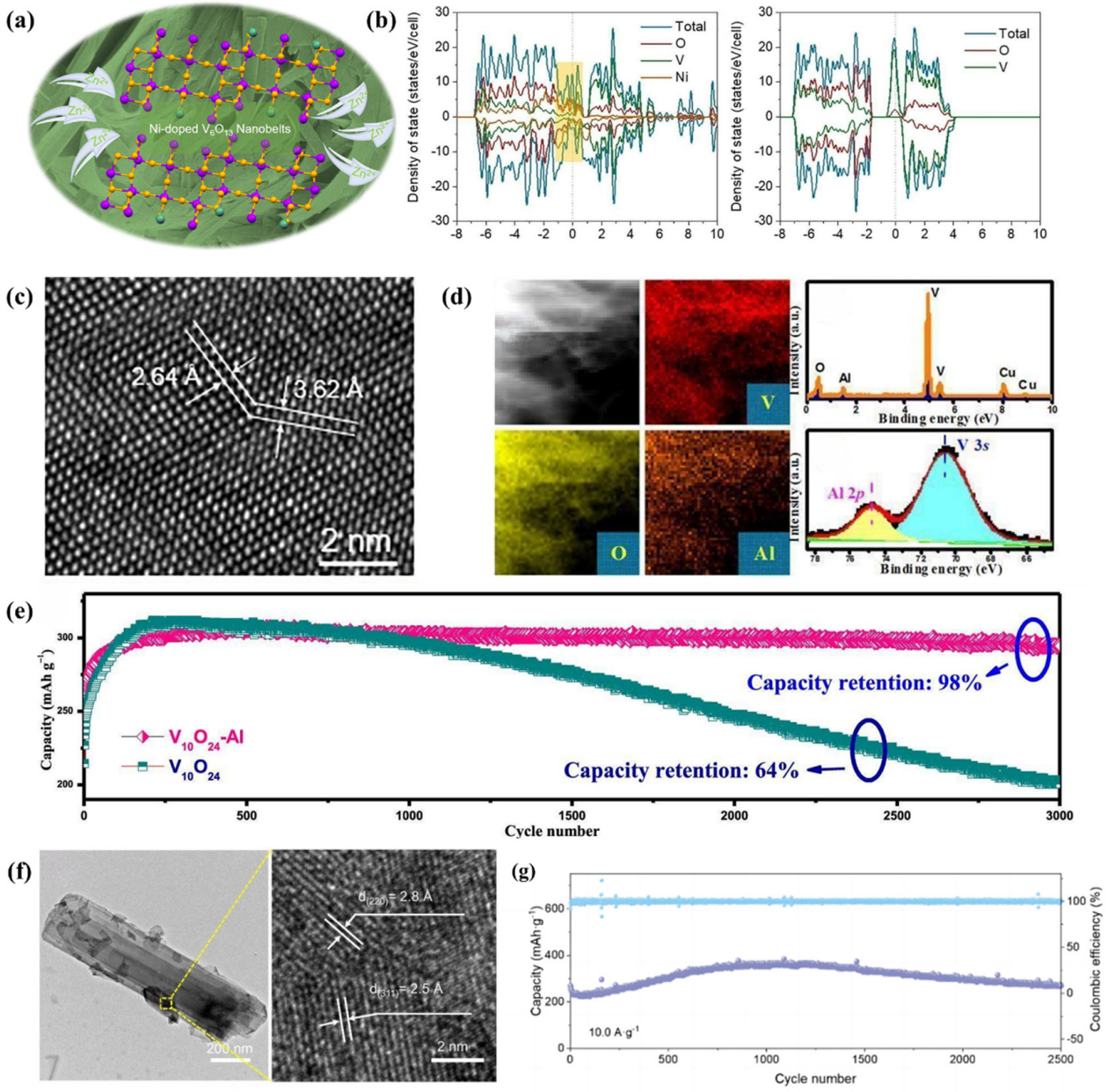

Figure 3. (**a**) Zn^{2+} storage diagram of $Ni_xV_{6-x}O_{13}$ cathode material (Ref. [39]). (**b**) Density of states (DOSs) of $Ni_xV_{6-x}O_{13}$ and V_6O_{13} are calculated by density function theory (DFT) (Ref. [39]). (**c**) High-resolution transmission electronic microscopy (HRTEM) images of $Ni_xV_{6-x}O_{13}$ (Ref. [39]). (**d**) Element mapping images, energy dispersive X-ray (EDX) spectra and X-ray photoelectron spectroscopy (XPS) spectra of Al-doped $V_{10}O_{24}$ (Ref. [40]). (**e**) Long-term cycling performance of $V_{10}O_{24}$ and $V_{10}O_{24}$-Al (Ref. [40]). (**f**) Scanning electronic microscopy (SEM), transmission electronic microscopy (TEM), and HRTEM images of VO_2@NC (Ref. [49]). (**g**) Long cycle performance of VO_2@NC (Ref. [49]).

Table 2. Performance comparison of vanadium oxide-based materials doped with different metal ions.

Cathode	Electrolyte	Specific Capacity (Current Density)	Cyclic Stability (Cycles, Current Density)	Ref.
Ag-doped V_2O_5	2M $Zn(CF_3SO_3)_2$	418 mAh g^{-1} (0.1 A g^{-1})	~100% (700, 3.0 A g^{-1})	[41]
Fe-doped V_2O_5	3M $Zn(CF_3SO_3)_2$	214 mAh g^{-1} (0.5 A g^{-1})	94.6% (300, 0.5 A g^{-1})	[42]
Mn-doped V_2O_5	1M $Zn(ClO_4)_2$	367 mAh g^{-1} (0.1 A g^{-1})	~140% (3000, 2.0 A g^{-1})	[43]
Al-doped $V_{10}O_{24}{\cdot}12H_2O$	3M $Zn(CF_3SO_3)_2$	355 mAh g^{-1} (1.0 A g^{-1})	98% (3000, 5.0 A g^{-1})	[40]
La-doped V_2O_5	1M $Zn(CF_3SO_3)_2$	405 mAh g^{-1} (0.1 A g^{-1})	93.8% (5000, 10.0 A g^{-1})	[44]
Ti-doped $NH_4V_4O_{10}$	3M $Zn(CF_3SO_3)_2$	298 mAh g^{-1} (0.1 A g^{-1})	89.02% (2000, 2.0 A g^{-1})	[45]
Sn-doped hydrated V_2O_5	3M $Zn(CF_3SO_3)_2$	373 mAh g^{-1} (0.1 A g^{-1})	87.2% (2500, 87.2 A g^{-1})	[46]
Ni-doped V_6O_{13}	3M $Zn(CF_3SO_3)_2$	302.6 mAh g^{-1} (1.0 A g^{-1})	96.5% (10,000, 8.0 A g^{-1})	[39]
W-doped VO_2	3M $Zn(CF_3SO_3)_2$	346 mAh g^{-1} (0.1 A g^{-1})	76.4% (1000, 4.0 A g^{-1})	[47]
K-doped VO_2(B)	3M $Zn(CF_3SO_3)_2$	376 mAh g^{-1} (0.5 A g^{-1})	80% (3000, 20.0 A g^{-1})	[48]

Non-metallic heteroatom doping is another effective doping method. Non-metallic heteroatom doping usually introduces elements such as nitrogen, phosphorus, sulfur, or fluorine into carbon-based or conductive polymer materials compounded with vanadium oxide-based materials. The doping of elements with high electronegative enhances the binding force between the composite materials, which effectively improves the cycle stability and rate performance of the cathode [50]. Lv et al. synthesized VO_2 with an N-doped amorphous carbon (VO_2@NC) by annealing the polydopamine-coated V_6O_{13} in argon at a high temperature (Figure 3f) [49]. VO_2@NC composites had abundant active sites, fast electron/ion transport rates, and amazing structural stabilities. Therefore, the VO_2@NC composite could maintain 99.7 % capacity after long cycles at a high current density (Figure 3g)

3.2. Vacancy Engineering

Vacancy engineering can adjust the electron distribution in vanadium oxide-based materials, which is an important strategy to optimize the electrochemical performance of vanadium oxide-based cathodes. Here, we divide vacancy engineering into cation vacancies and anion vacancies, according to the type of introduced vacancies.

3.2.1. Anion Vacancies

The introduction of anion vacancies is an effective strategy for tuning the electrochemical performance of the AZIB cathode. The most common forms of anion vacancies in vanadium oxide-based materials are oxygen vacancies. The formation of oxygen defects usually requires the material to be treated in a reducing environment [51,52]. It is a common method to introduce oxygen vacancies by placing vanadium oxide-based materials into a $NaBH_4$ solution with a strong reducibility. Zhang et al. prepared VO_{2-x}(B) with oxygen vacancies by reacting VO_2(B) with a $NaBH_4$ solution (Figure 4a–c) [53]. Due to the presence of oxygen vacancies, VO_{2-x}(B) exhibited excellent specific capacity and cycle stability. At a high temperature, the reducing atmosphere (mixture of H_2 and inert gas, etc.) can also provide the environment required for vacancy generation. Liao et al. synthesized oxygen vacancy-rich V_6O_{13} (O_d-VO) by annealing nano-textile-like V_6O_{13} at 250 °C in a H_2/N_2 mixed atmosphere for 3 h (Figure 4d) [54]. The presence of oxygen vacancies brought more Zn^{2+}-embedded active sites, resulting in an increase in the specific capacity (Figure 4e). Through electrochemical performance and simulation, it was found that the introduction of oxygen vacancies could effectively improve the structural stability of V_6O_{13} in the Zn^{2+} insertion/extraction process (Figure 4f). In addition, the assembled flexible Zn/O_d-VO battery achieved good mechanical properties due to the absence of binders in the cathode.

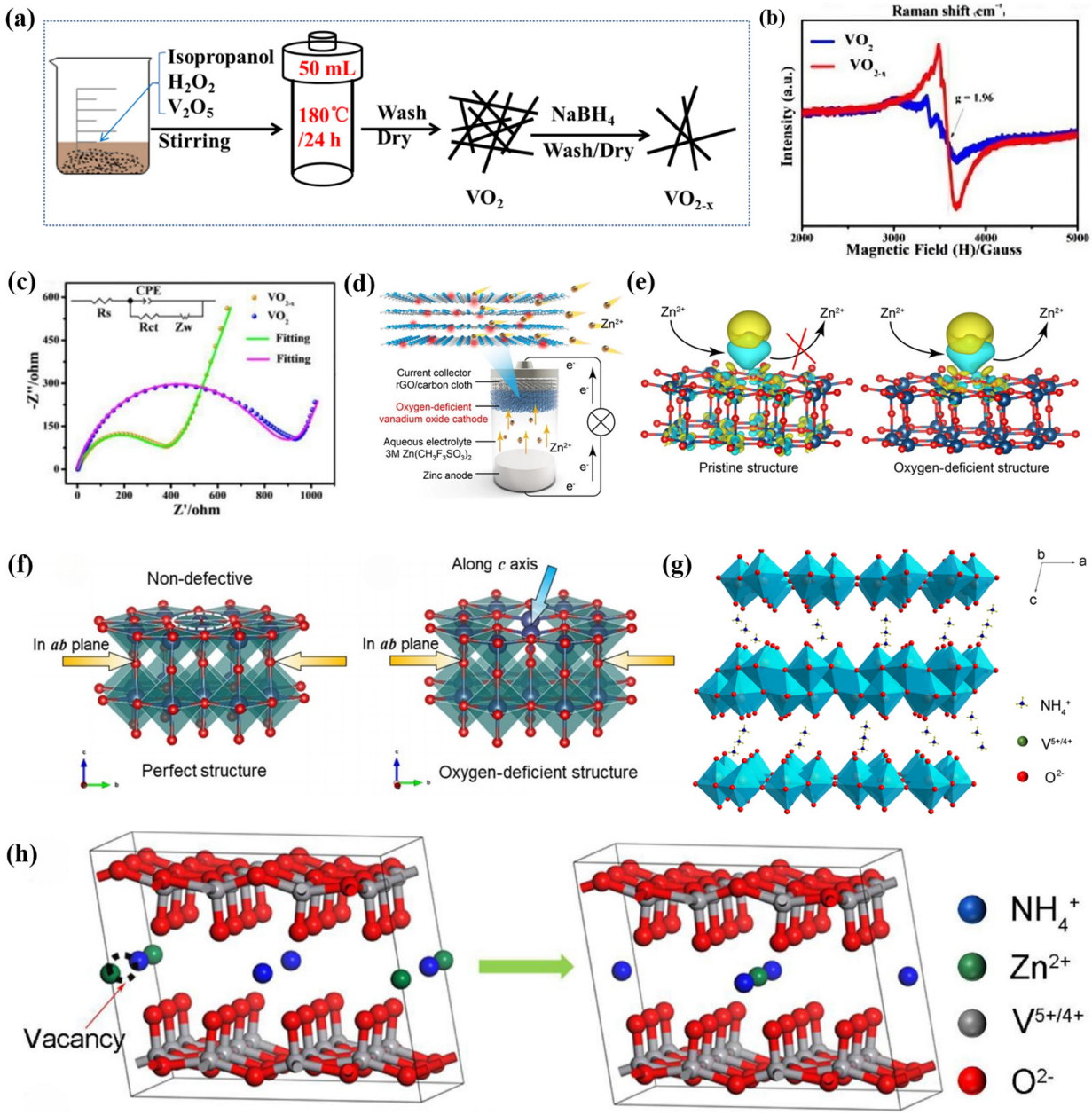

Figure 4. (**a**) Preparation flow chart of VO_2 and VO_{2-x} (Ref. [53]). (**b**) Electron paramagnetic resonance (EPR) spectra of VO_2 and VO_{2-x} (Ref. [53]). (**c**) Nyquist diagram of VO_2 and VO_{2-x} (Ref. [53]). (**d**) Structure and discharge process of Zn/O_d-VO battery (Ref. [54]). (**e**) Zn^{2+} acceptance/release model of V_6O_{13} before and after modification (Ref. [54]). (**f**) The charge distribution and corresponding structure of p-VO and O_d-VO (Ref. [54]). (**g**) Crystal structure diagram of $NH_4V_4O_{10}$ (Ref. [55]). (**h**) Diffusion diagram of Zn^{2+} in ZNV with NH^{4+} interlayer vacancy (Ref. [55]).

3.2.2. Cation Vacancies

Cation vacancies can also be introduced into vanadium oxide-based cathode materials to improve their electrochemical performance. However, unlike oxygen vacancies, the generation of cation vacancies in vanadium oxide-based materials is usually accompanied by the introduction of guest species. For example, He et al. introduced Zn^{2+} as a pre-intercalated guest species by a two-step hydrothermal method and a $Zn_{0.3}(NH_4)_{0.3}V_4O_{10}{\cdot}0.91H_2O$ (ZNV) cathode material with a large number of cation vacancies was prepared (Figure 4g) [55]. The existence of cation vacancies was beneficial to the diffusion of Zn^{2+} and provided a significant number of active sites embedded

by Zn^{2+} (Figure 4h). In addition, Zn^{2+}, NH^{4+}, and structural water molecules acted as interlayer pillars to improve structural stability. The interlayer water molecules alleviated the electrostatic interaction during the electrochemical reaction and achieved the effect of charge shielding [18].

3.3. Interlayer Engineering

The pre-intercalation strategy is a very promising method for the modification of vanadium oxide-based materials. The guest species introduced into the interlayer can form strong ionic bonds or hydrogen bonds with the host material to prevent interlayer slip and structural collapse, thereby effectively suppressing structural degradation [56]. In addition, pre-intercalation can also expand the interlayer distance of the host materials, which promotes the ion diffusion kinetics of Zn^{2+} in vanadium oxide-based materials [57]. According to different guest species, we divide the pre-intercalation into: (1) molecular pre-intercalation and (2) cation pre-intercalation.

3.3.1. Molecules Pre-Intercalation

Small molecules such as H_2O and CO_2 can be supported between the layers of vanadium oxide-based materials, while optimizing the cycle life and ion transport of the cathode, thereby obtaining excellent cycle performances and rate performances [24]. Yan et al. reported $V_2O_5{\cdot}nH_2O$ with structural water molecules. Structural water molecules could be used as shielding media, which reduces the effective charge of Zn^{2+} and optimizes the ion transport rate (Figure 5a) [18]. The cycle stability of $V_2O_5{\cdot}nH_2O$ was significantly improved compared with V_2O_5 without interlayer crystal water. In the pre-intercalation strategy, CO_2 can also be introduced into the interlayer as a guest species. Shi et al. creatively synthesized CO_2-intercalated V_6O_{13} by decomposing oxalic acid in the framework of hydrated V_6O_{13} (Figure 5b) [58]. Due to the Coulomb interaction between O_{CO2} and Zn^{2+}, the path diffusion barrier of Zn^{2+} was significantly reduced, which promoted the improvement of the cycle stability and rate performance.

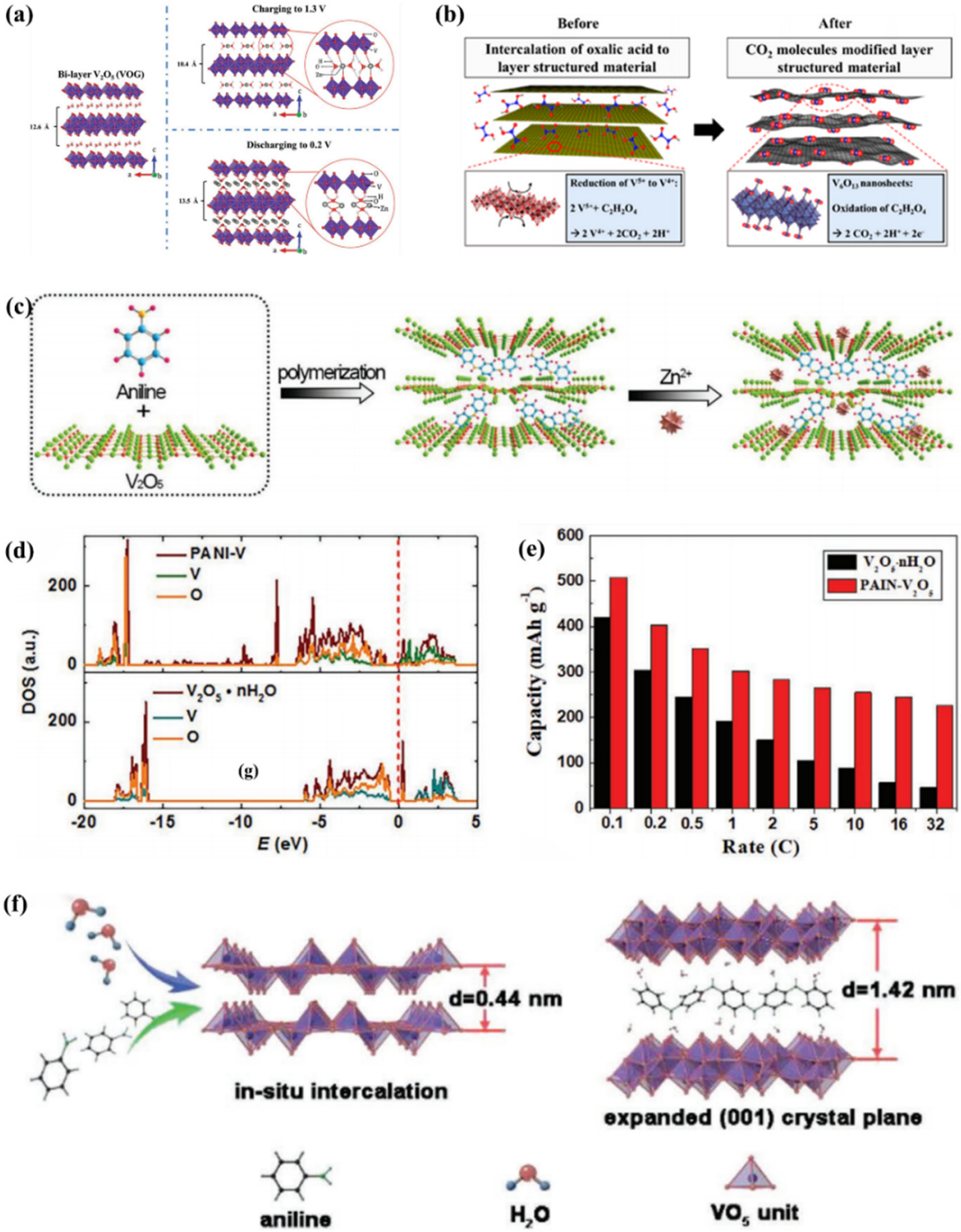

Figure 5. (**a**) The crystal structure of the original VOG and the VOG after charge and discharge (Ref. [18]). (**b**) The structure diagram of V_6O_{13} before and after CO_2 molecule embedding (Ref. [58]). (**c**) Preparation of PANI-V superlattice material (Ref. [59]). (**d**) DOS of $V_2O_5 \cdot nH_2O$ and PANI-V (Ref. [59]). (**e**) Rate capacity of PANI-V (Ref. [59]). (**f**) The schematic diagram of PANI-intercalated V_2O_5 (Ref. [60]).

Although H_2O or CO_2 molecules can be embedded in the crystal framework as pillars, the pillars are irreversibly removed during charging and discharging due to the weak binding force between the molecules and the lattice skeleton. Recently, conductive

polymers (polyaniline (PANI), polypyrrole (PPy), and poly(3,4-ethylenedioxythiophene) (PEDOT), etc.) have been embedded as guest species into the interlayer of vanadium oxide-based materials [61–63]. The presence of conductive polymers promotes the electron/ion transport rate of the cathode, resulting in better rates and cycle performances. Li et al. obtained PANI-V_2O_5 by embedding PANI as the guest species (Figure 5c) [59]. PANI was connected to the host material through hydrogen bonds between the -NH_2 group and the V-O layer, and PANI acted as a pillar to obtain a super high-rise spacing of 15.6 Å for the AZIB cathode. In addition, the electron transport rates of the cathode material can be improved by introducing a conductive polymer (PANI) (Figure 5d). The large number of interfaces in PANI-V changed the charge distribution and the structure inside the cathode material, weakening the Coulomb force between Zn^{2+} and the host framework. Therefore, PANI-V had an excellent rate capability and capacity retention (Figure 5e). Similarly, Chen et al. intercalated PANI in situ into V_2O_5 by a hydrothermal method to improve the battery performance (Figure 5f) [60]. The flexibility of the conjugated polymer chain alleviated the structural stress of the confined layer during the Zn^{2+} deintercalation process, thereby improving the cycle stability.

3.3.2. Cation Pre-Intercalation

Metal cations usually have unique d-orbital electrons [64]. Pre-embedding different metal cations into vanadium oxide-based materials can inhibit structural collapse and promote the electron/ion transport rate of the cathode. For example, Yang et al. reported that different metal cations (Fe^{2+}, Co^{2+}, Ni^{2+}, Mn^{2+}, Zn^{2+}, and Cu^{2+}) were intercalated into V_2O_5 to obtain $M_xV_2O_5$ cathode materials (Figure 6a,b) [65]. Compared with unmodified V_2O_5, $M_xV_2O_5$ had a higher Zn^{2+} transport rate and cycle stability (Figure 6c).

The radius of metal ions is a critical factor affecting the degree of pre-intercalation. The difficulty of embedding metal ions increases with the increase of the radius [56]. The introduction of metal ions with large radii can be used as interlayer pillars to suppress volume change, increase interlayer spacing and improve the Zn^{2+} transmission rate. However, interlayer ions with large radii may hinder the intercalation of Zn^{2+} and reduce the capacity [66]. In addition, the introduction of ions with too large radius also can destroy the interaction force between layers, resulting in structural instability and the decline of the cycle performance.

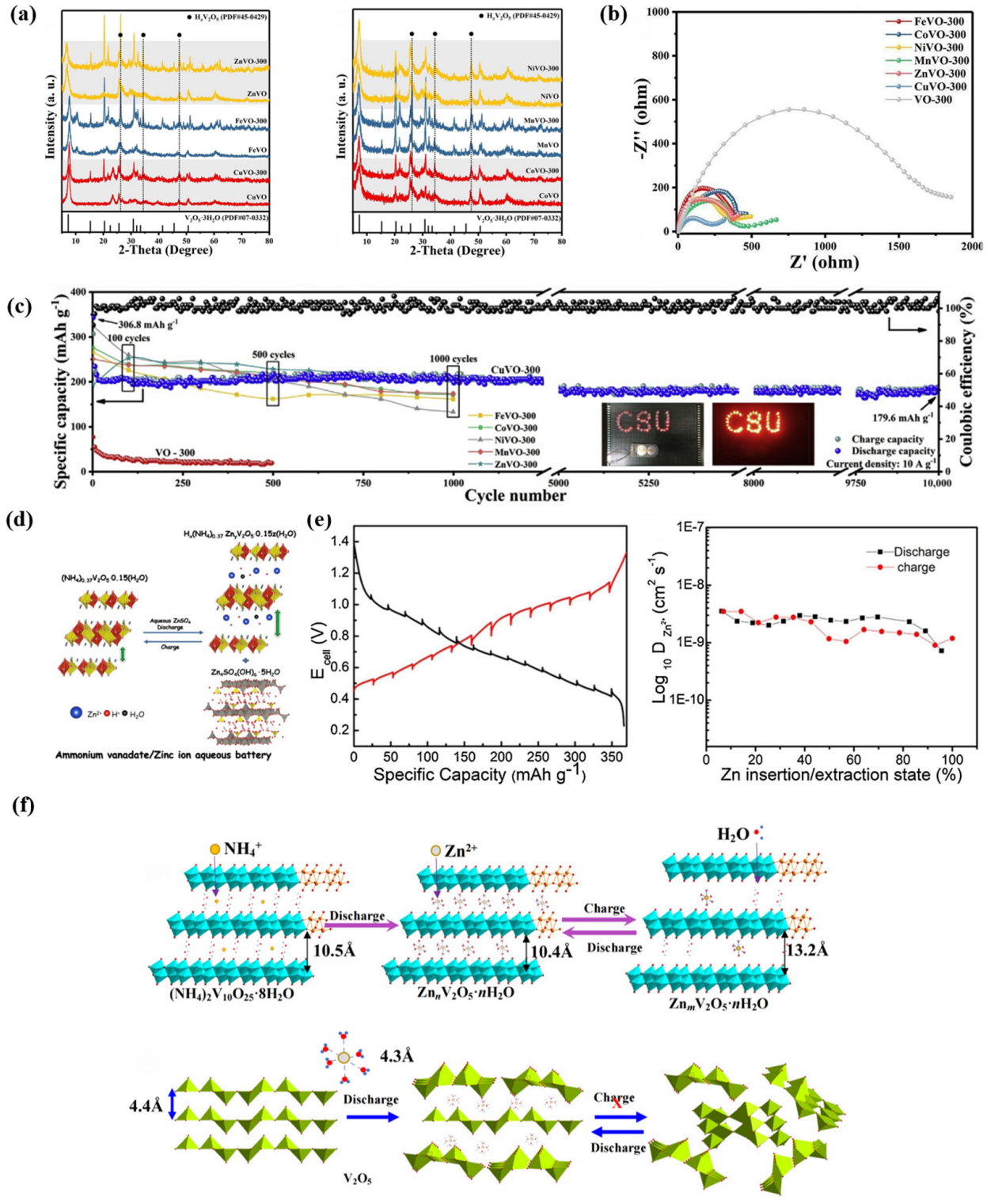

Figure 6. (**a**) X-ray diffraction (XRD) patterns of Cu/Fe/Zn/Co/Mn/NiVO-0/300 (Ref. [65]). (**b**) Electrochemical Impedance Spectroscopy (EIS) of TVO-300 and VO-300 (Ref. [65]). (**c**) Long-term cycling performance of TVO-300 and VO-300 (Ref. [65]). (**d**) The structure diagram of $(NH_4)_{0.37}V_2O_5{\cdot}0.15H_2O$ during the charge and discharge processes (Ref. [67]). (**e**) Diffusion coefficients of Zn^{2+} calculated from galvanostatic intermittent titration technique (GITT) (Ref. [67]). (**f**) Structural changes of $(NH_4)_2V_{10}O_{25}{\cdot}8H_2O$ during Zn insertion/extraction (Ref. [68]).

NH^{4+}, as a small inorganic ion, is also often used as a pre-embedded guest cation. The radius of the inserted NH^{4+} (1.48 Å) is larger than the radius of the zinc ion (0.75 Å), which guarantees a high transport rate during Zn^{2+} insertion [69]. In addition, due to the hydrogen bond between NH^{4+} and the lattice oxygen ions of vanadium oxide-based materials, NH^{4+} is firmly combined with the main framework of vanadium oxides, which optimizes the structural stability and alleviates the dissolution of the cathode. Compared with metal ions, NH^{4+} has a lower molar mass, which can alleviate the loss of specific capacity caused by the introduction of guest species. Tamilselvan et al. synthesized $(NH_4)_{0.37}V_2O_5{\cdot}0.15H_2O$ nanoflowers as cathode materials for AZIBs. (Figure 6d) [67]. The intercalation of NH^{4+} resulted in a large interlayer spacing of 11.85 Å for $(NH_4)_{0.37}V_2O_5{\cdot}0.15H_2O$, which greatly promoted the transport rate of Zn^{2+} (Figure 6e). In addition, Wei et al. used ultrathin $(NH_4)_2V_{10}O_{25}{\cdot}8H_2O$ nanobelts as cathode materials for AZIBs (Figure 6f) [68]. $(NH_4)_2V_{10}O_{25}{\cdot}8H_2O$ had a very high controllable interlayer spacing, which could be adjusted between 10.45~13.2Å. The high Zn^{2+} transport rate was achieved due to the unique ultra-thin stable structure and large interlayer spacing.

3.4. Structural Composite

3.4.1. Coating

In general, vanadium oxide-based materials have low intrinsic conductivities, and structural deterioration during charging and discharging causes capacity decline [70]. Surface coating is a typical strategy to optimize the structural stability of vanadium oxide-based cathodes. It can be used as a barrier between the vanadium oxide and the electrolyte to protect the cathode. The surface coating inhibits the side reactions at the cathode and electrolyte interface, which improve the cycle stability of the cathode. In addition, the introduction of carbon-based materials and conductive polymers as surface coatings can significantly improve the electrical conductivity, thereby achieving rapid reaction kinetics of the cathode [71,72].

Amorphous carbon coating has been widely used in vanadium oxide-based materials due to its significantly improved conductivity of the cathode, which promotes electron transfer during the redox reaction. For example, Zhang et al. synthesized N-doped carbon/V_2O_3 composite fibers as cathode materials for AZIB by electrospinning and high temperature carbonization (Figure 7a) [73]. V_2O_3 nanoparticles were encapsulated in an amorphous carbon skeleton, which significantly improved the electron transport rate of V_2O_3. Moreover, the presence of a carbon skeleton improved the structural degradation problem and alleviated the capacity decay during the cycle. In addition to amorphous carbon, graphene and carbon nanotubes can also be combined with vanadium oxide-based materials. Pang et al. prepared a graphene-coated $H_2V_3O_8$ composite as a cathode material for AZIBs (Figure 7b) [74]. Due to the high electron transfer rate of graphene, the $H_2V_3O_8$/graphene cathode exhibited an excellent rate performance. The graphene sheet acted as an elastic skeleton of $H_2V_3O_8$ to alleviate the dissolution of the cathode material during the cycle, which greatly improved the cycle stability of the cathode (Figure 7c).

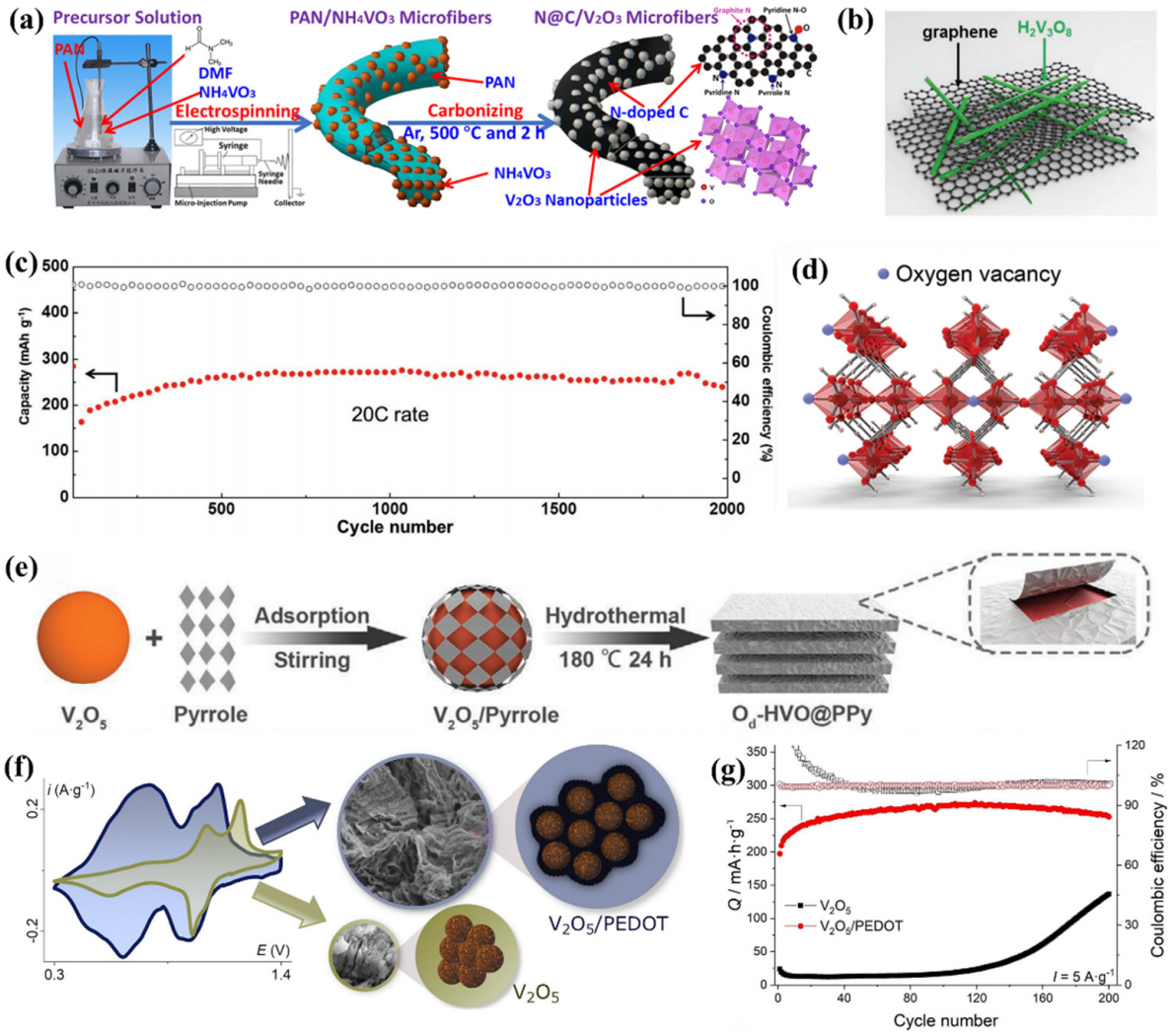

Figure 7. (**a**) Synthesis and structure of N@C/V_2O_3 composites (Ref. [73]). (**b**) Structural sketch of $H_2V_3O_8$ NW/graphene composite material (Ref. [74]). (**c**) Long cycle stability of $H_2V_3O_8$ NW/graphene composite material at 20 C rate (Ref. [74]). (**d**) Crystal structure diagram of O_d-VO_2·xH_2O (Ref. [75]). (**e**) Schematic diagram of preparation process of O_d–HVO@PPy nanosheets (Ref. [75]). (**f**) Diagram of V_2O_5 and V_2O_5/PEDOT [76]. (**g**) Cycle performance of V_2O_5 and V_2O_5/PEDOT (Ref. [76]).

Organic polymer coating is another effective method for optimizing electrochemical performance in addition to coating with carbon-based materials. For example, Zhang et al. synthesized an anoxic VO_2 hydrate (O_d-HVO@PPy) with PPY coating by a hydrothermal reaction (Figure 7d,e) [75]. The presence of conductive polymers improved the conductivity of the cathode and inhibited the dissolution of vanadium during the cycle. In addition, embedding crystal water in the VO_2 tunnel structure could expand the tunnel size and alleviated the Coulomb interaction between Zn^{2+} and the V-O framework [18]. The O_d-HVO@PPy cathode material exhibited an excellent structural stability and cycle stability. Volkov et al. obtained V_2O_5 with poly (3,4-ethylenedioxythiophene) (V_2O_5/PEDOT) coating as the cathode material for AZIBs by the chemical oxidation of EDOT (Figure 7f) [76]. Compared with the unmodified V_2O_5, V_2O_5/PEDOT exhibited an excellent rate performance and an amazing cycle stability (Figure 7g).

3.4.2. Heterostructure

When there are different phases in the AZIB cathode material, a built-in electric field is generated at the phase interface because of the difference in the work function of the heterostructure interface [77]. During the electrochemical reaction, Zn^{2+} moves in the direction of the built-in electric field. This significantly reduces the diffusion barrier of Zn^{2+}, which promotes the transmission efficiency of Zn^{2+}. Moreover, the heterostructure can also cause the redistribution of charge on both sides of the interface, change the structure and distribution of charge inside the cathode material, and optimize the conductivity of the cathode. The simultaneous change of the electron/ion transport rate and diffusion distance makes AZIBs obtain better rate performances. Chen et al. synthesized VO_2@V_2C heterostructure by hydrothermal reaction (Figure 8a) [78]. The generation of heterostructures shortened the diffusion size of Zn^{2+} and promoted the electron transport of VO_2 (Figure 8b). Finally, the rate performance of VO_2 was effectively improved (Figure 8c). In addition, Zhao et al. synthesized a-V_2O_5@$Ti_3C_2T_x$ heterostructure by the in situ assembly of amorphous V_2O_5 and $Ti_3C_2T_x$ MXene (Figure 8d) [79]. Under the synergistic effect of a-V_2O_5 and $Ti_3C_2T_x$ Mxene, the a-V_2O_5@Ti_3C_2T heterostructure obtained abundant active sites, excellent electron/ion transport rates, and isotropic ion diffusion pathways. Finally, a-V_2O_5@Ti_3C_2T exhibited an amazing specific capacity, rate performance, and cycle stability (Figure 8e).

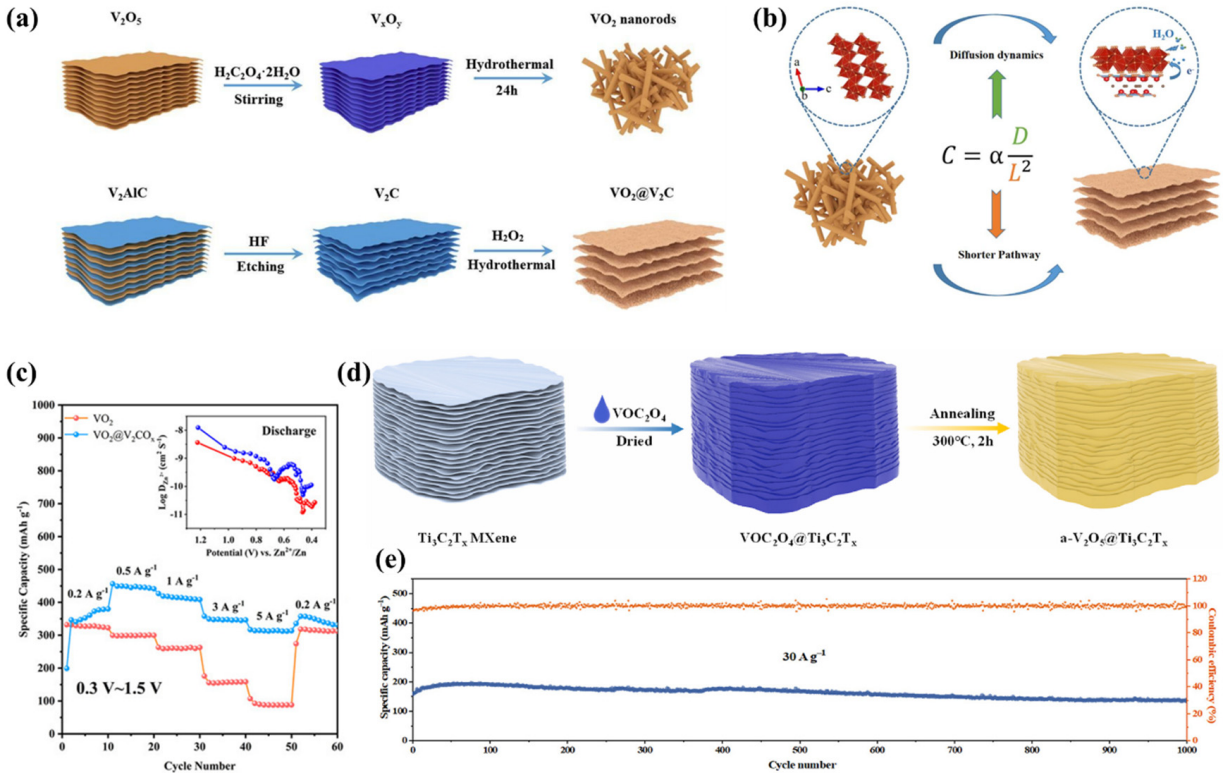

Figure 8. (**a**) Preparation process chart of VO_2 nanorods and VO_2@V_2C (Ref. [78]). (**b**) The rate performance improvement diagram of VO_2@V_2C relative to VO_2 (Ref. [78]). (**c**) Rate performance diagrams for VO_2 and VO_2@V_2C (Ref. [78]). (**d**) Synthesis schematic of a-V_2O_5@$Ti_3C_2T_x$ (Ref. [79]). (**e**) Long cycle performance of a-V_2O_5 @ $Ti_3C_2T_x$ (Ref. [79]).

Recently, other optimization strategies for some vanadium oxide-based cathode materials have been effectively developed. For example, Zhu et al. in situ electrochemically oxidized VO_2 nanorods to $V_2O_5{\cdot}1.75H_2O$ at a high anodic potential as AZIB cathode materials [80]. Due to the structural similarity between VO_2 and $V_2O_5{\cdot}1.75H_2O$, the surface electrochemical reaction was enhanced by adaptively adjusting the lattice structure during

the electrochemical activation process, so that the cathode obtained an excellent electrochemical performance. In addition, Wu et al. synthesized vanadium oxides with different crystal structures from different V^{5+} solute species by controlling the pH value of the precursor solution [81]. The $Zn_{0.15}V_2O_5{\cdot}0.76H_2O$ bilayer structure with a large interplanar spacing of 14.0 Å was obtained by adjusting the pH value. This provided a large number of active sites for Zn^{2+} insertion/extraction and achieved rapid ion transport kinetics. The discovery and proposal of these strategies further enriches the research direction of AZIB cathode materials, which greatly promotes the progress and development of AZIBs.

4. Summary and Perspectives

Recently, the development of vanadium oxide-based aqueous AZIBs has made great progress in terms of the synthesis, characterization, and performance. Vanadium oxide-based aqueous AZIBs exhibit excellent electrochemical performances because of their rich oxidation state species and open structures. This paper summarizes various methods, such as substitutional doping, vacancy engineering, interlayer engineering, and structural composite, for optimizing the performance of vanadium oxide-based cathodes. Although great achievements have been made in vanadium oxide-based cathode materials in recent years, several issues should be carefully considered for more advanced aqueous AZIBs in the future.

1. Find the right object species. The dissolution and collapse of vanadium oxide-based materials during electrochemical reactions always destroy their cyclic stability, making it difficult for vanadium oxide-based materials to achieve large-scale commercial applications. Finding suitable guest species as interlayer pillars is the key to effectively improve the structural stability. In addition, the pre-embedded amount of guest species also has a considerable impact on the structural stability.
2. Explore new methods to inhibit the formation of zinc dendrites. The anode material is one of the crucial parts of the battery system, which has a significant impact on the performance of AZIBs [82,83]. The zinc dendrite problem is a major challenge for AZIB anode materials. The presence of zinc dendrites can lead to a decrease in the battery life. Surface modification and regulation of zinc deposition and dissolution behavior are common strategies for the study of zinc anodes [84,85]. For example, Chen inhibited dendrite formation by covering the polyacrylonitrile coating on the zinc anode [85]. In addition, we urgently need to find new strategies to solve the problem of zinc dendrite growth.
3. Explore new electrolyte additives and their mechanisms. The use of aqueous electrolyte makes AZIBs much safer than LIBs. However, the presence of solvent water in aqueous electrolytes also leads to many side reactions, which have a negative impact on the reversibility of electrochemical reactions [86]. The electrolyte additives can stabilize the positive and negative structures at the same time and eliminate the adverse side reactions during the reaction [1,87]. Cao et al. introduced sulfolane (SL) into the $ZnSO_4$ electrolyte, which inhibited zinc dendrite growth and side reactions [87]. In addition, the compatibility of electrolytes with cathode and anode materials should also be considered in the modification of electrolytes.
4. Development of more advanced non-electrode components. The significant progress in the field of AZIBs not only benefits from the rapid development of electrode materials, but also requires efforts in non-electrode components (current collectors, binders, separators, etc.) [88]. For example, Li et al. developed a waste palm lignocellulose nanofiber (LCNF) separator, which improved the kinetics of zinc deposition and effectively inhibited the growth of zinc dendrites [89]. Each battery is a system formed by the synergy of electrode materials and non-electrode components. The compatibility between electrode materials and non-electrode components determines the efficiency of the battery. Advanced non-electrode components enable AZIBs to achieve a higher energy and power density, which is expected to promote the further development of AZIBs.

5. Develop advanced AZIB recycling technology. Although most vanadium oxide-based AZIBs have the characteristic of low toxicity, they still have potential hazards to the environment when they are widely used as AZIB cathode materials in various energy storage systems [90]. Hence, it is meaningful to develop a new recovery technology with a simple process and a low cost. In addition, the recovery of Ti and other metals in zinc-ion batteries can further reduce the production costs and improve economic efficiency. Therefore, it is urgent to develop an effective AZIB recycling technology to form a green, safe, and sustainable production cycle chain to further promote the progress and development of AZIBs.

Author Contributions: Writing—original draft preparation, Y.Q.; writing—review and editing, Z.G. and Z.Y.; formal analysis, P.W. and B.D.; data curation, Z.S. and H.L.; supervision, L.Q.; investigation, S.T. and H.D. All authors have read and agreed to the published version of the manuscript.

Funding: This research received no external funding.

Institutional Review Board Statement: Not applicable.

Informed Consent Statement: Not applicable.

Data Availability Statement: Not applicable.

Conflicts of Interest: The authors declare no conflict of interest.

References

1. Pan, H.L.; Shao, Y.Y.; Yan, P.F.; Cheng, Y.W.; Han, K.S.; Nie, Z.M.; Wang, C.M.; Yang, J.H.; Li, X.L.; Bhattacharya, P.; et al. Reversible aqueous zinc/manganese oxide energy storage from conversion reactions. *Nat. Energy* **2016**, *1*, 16039. [CrossRef]
2. Dunn, B.; Kamath, H.; Tarascon, J.-M. Electrical Energy Storage for the Grid: A Battery of Choices. *Science* **2011**, *334*, 928–935. [CrossRef]
3. Gielen, D.; Boshell, F.; Saygin, D.; Bazilian, M.D.; Wagner, N.; Gorini, R. The role of renewable energy in the global energy transformation. *Energy Strategy Rev.* **2019**, *24*, 38–50. [CrossRef]
4. Luo, X.; Wang, J.; Dooner, M.; Clarke, J. Overview of current development in electrical energy storage technologies and the application potential in power system operation. *Appl. Energy* **2015**, *137*, 511–536. [CrossRef]
5. Armand, M.; Tarascon, J.M. Building better batteries. *Nature* **2008**, *451*, 652–657. [CrossRef]
6. Larcher, D.; Tarascon, J.M. Towards greener and more sustainable batteries for electrical energy storage. *Nat. Chem.* **2015**, *7*, 19–29. [CrossRef]
7. Tarascon, J.M. Is lithium the new gold? *Nat. Chem.* **2010**, *2*, 510. [CrossRef]
8. Ponrouch, A.; Bitenc, J.; Dominko, R.; Lindahl, N.; Johansson, P.; Palacin, M.R. Multivalent rechargeable batteries. *Energy Storage Mater.* **2019**, *20*, 253–262. [CrossRef]
9. Song, M.; Tan, H.; Chao, D.L.; Fan, H.J. Recent Advances in Zn-Ion Batteries. *Adv. Funct. Mater.* **2018**, *28*, 1802564. [CrossRef]
10. Liu, W.B.; Hao, J.W.; Xu, C.J.; Mou, J.; Dong, L.B.; Jiang, F.Y.; Kang, Z.; Wu, J.L.; Jiang, B.Z.; Kang, F.Y. Investigation of zinc ion storage of transition metal oxides, sulfides, and borides in zinc ion battery systems. *Chem. Commun.* **2017**, *53*, 6872–6874. [CrossRef] [PubMed]
11. Vernardou, D.; Drosos, H.; Spanakis, E.; Koudoumas, E.; Katsarakis, N.; Pemble, M.E. Electrochemical properties of amorphous WO_3 coatings grown on polycarbonate by aerosol-assisted CVD. *Electrochim. Acta* **2012**, *65*, 185–189. [CrossRef]
12. Wan, F.; Zhang, Y.; Zhang, L.; Liu, D.; Wang, C.; Song, L.; Niu, Z.; Chen, J. Reversible Oxygen Redox Chemistry in Aqueous Zinc-Ion Batteries. *Angew. Chem.-Int. Ed.* **2019**, *58*, 7062–7067. [CrossRef] [PubMed]
13. Xu, C.; Li, B.; Du, H.; Kang, F. Energetic Zinc Ion Chemistry: The Rechargeable Zinc Ion Battery. *Angew. Chem.-Int. Ed.* **2012**, *51*, 933–935. [CrossRef]
14. Blanc, L.E.; Kundu, D.; Nazar, L.F. Scientific Challenges for the Implementation of Zn-Ion Batteries. *Joule* **2020**, *4*, 771–799. [CrossRef]
15. Kang, S.; Reeves, K.G.; Koketsu, T.; Ma, J.; Borkiewicz, O.J.; Strasser, P.; Ponrouch, A.; Dambournet, D. Multivalent Mg^{2+}-, Zn^{2+}-, and Ca^{2+}-Ion Intercalation Chemistry in a Disordered Layered Structure. *Acs Appl. Energy Mater.* **2020**, *3*, 9143–9150. [CrossRef]
16. Daskalakis, S.; Wang, M.; Carmalt, C.J.; Vernardou, D. Electrochemical Investigation of Phenethylammonium Bismuth Iodide as Anode in Aqueous Zn_{2+} Electrolytes. *Nanomaterials* **2021**, *11*, 656. [CrossRef] [PubMed]
17. Liu, Y.; He, G.; Jiang, H.; Parkin, I.P.; Shearing, P.R.; Brett, D.J.L. Cathode Design for Aqueous Rechargeable Multivalent Ion Batteries: Challenges and Opportunities. *Adv. Funct. Mater.* **2021**, *31*, 2010445. [CrossRef]
18. Yan, M.; He, P.; Chen, Y.; Wang, S.; Wei, Q.; Zhao, K.; Xu, X.; An, Q.; Shuang, Y.; Shao, Y. Water-Lubricated Intercalation in $V_2O_5{\cdot}nH_2O$ for High-Capacity and High-Rate Aqueous Rechargeable Zinc Batteries. *Adv. Mater.* **2017**, *30*, 1703725. [CrossRef] [PubMed]

19. Zhao, X.; Liang, X.; Li, Y.; Chen, Q.; Chen, M. Challenges and design strategies for high performance aqueous zinc ion batteries. *Energy Storage Mater.* **2021**, *42*, 533–569. [CrossRef]
20. Ding, J.; Gao, H.; Ji, D.; Zhao, K.; Wang, S.; Cheng, F. Vanadium-based cathodes for aqueous zinc-ion batteries: From crystal structures, diffusion channels to storage mechanisms. *J. Mater. Chem. A* **2021**, *9*, 5258–5275. [CrossRef]
21. Chen, X.; Wang, L.; Li, H.; Cheng, F.; Chen, J. Porous V_2O_5 nanofibers as cathode materials for rechargeable aqueous zinc-ion batteries. *J. Energy Chem.* **2019**, *38*, 20–25. [CrossRef]
22. Javed, M.S.; Lei, H.; Wang, Z.; Liu, B.-T.; Cai, X.; Mai, W. 2D V_2O_5 nanosheets as a binder-free high-energy cathode for ultrafast aqueous and flexible Zn-ion batteries. *Nano Energy* **2020**, *70*, 104573. [CrossRef]
23. Chen, L.; Ruan, Y.; Zhang, G.; Wei, Q.; Jiang, Y.; Xiong, T.; He, P.; Yang, W.; Yan, M.; An, Q.; et al. Ultrastable and High-Performance Zn/VO_2 Battery Based on a Reversible Single-Phase Reaction. *Chem. Mater.* **2019**, *31*, 699–706. [CrossRef]
24. Li, Z.; Ganapathy, S.; Xu, Y.; Zhou, Z.; Sarilar, M.; Wagemaker, M. Mechanistic Insight into the Electrochemical Performance of Zn/VO_2 Batteries with an Aqueous $ZnSO_4$ Electrolyte. *Adv. Energy Mater.* **2019**, *9*, 1900237. [CrossRef]
25. Wei, T.; Li, Q.; Yang, G.; Wang, C. An electrochemically induced bilayered structure facilitates long-life zinc storage of vanadium dioxide. *J. Mater. Chem. A* **2018**, *6*, 8006–8012. [CrossRef]
26. Chen, L.; Yang, Z.; Huang, Y. Monoclinic VO_2(D) hollow nanospheres with super-long cycle life for aqueous zinc ion batteries. *Nanoscale* **2019**, *11*, 13032–13039. [CrossRef]
27. Ding, J.; Zheng, H.; Gao, H.; Liu, Q.; Hu, Z.; Han, L.; Wang, S.; Wu, S.; Fang, S.; Chou, S. In Situ Lattice Tunnel Distortion of Vanadium Trioxide for Enhancing Zinc Ion Storage. *Adv. Energy Mater.* **2021**, *11*, 2100973. [CrossRef]
28. Luo, H.; Wang, B.; Wang, F.; Yang, J.; Wu, F.; Ning, Y.; Zhou, Y.; Wang, D.; Liu, H.; Dou, S. Anodic Oxidation Strategy toward Structure-Optimized V_2O_3 Cathode via Electrolyte Regulation for Zn-Ion Storage. *Acs Nano* **2020**, *14*, 7328–7337. [CrossRef]
29. Shin, J.; Choi, D.S.; Lee, H.J.; Jung, Y.; Choi, J.W. Hydrated Intercalation for High-Performance Aqueous Zinc Ion Batteries. *Adv. Energy Mater.* **2019**, *9*, 1900083. [CrossRef]
30. Zhang, S.; Tan, H.; Rui, X.; Yu, Y. Vanadium-Based Materials: Next Generation Electrodes Powering the Battery Revolution? *Acc. Chem. Res.* **2020**, *53*, 1660–1671. [CrossRef] [PubMed]
31. Zhou, J.; Shan, L.; Wu, Z.; Guo, X.; Fang, G.; Liang, S. Investigation of V_2O_5 as a low-cost rechargeable aqueous zinc ion battery cathode. *Chem. Commun.* **2018**, *54*, 4457–4460. [CrossRef] [PubMed]
32. Kundu, D.; Adams, B.D.; Duffort, V.; Vajargah, S.H.; Nazar, L.F. A high-capacity and long-life aqueous rechargeable zinc battery using a metal oxide intercalation cathode. *Nat. Energy* **2016**, *1*, 16119. [CrossRef]
33. Zhu, K.; Wu, T.; Sun, S.; van den Bergh, W.; Stefik, M.; Huang, K. Synergistic H^+/Zn^{2+} dual ion insertion mechanism in high-capacity and ultra-stable hydrated VO_2 cathode for aqueous Zn-ion batteries. *Energy Storage Mater.* **2020**, *29*, 60–70. [CrossRef]
34. Lai, J.; Zhu, H.; Zhu, X.; Koritala, H.; Wang, Y. Interlayer-Expanded $V_6O_{13}{\cdot}nH_2O$ Architecture Constructed for an Advanced Rechargeable Aqueous Zinc-Ion Battery. *Acs Appl. Energy Mater.* **2019**, *2*, 1988–1996. [CrossRef]
35. Li, Y.; Zhang, D.; Huang, S.; Yang, H.Y. Guest-species-incorporation in manganese/vanadium-based oxides: Towards high performance aqueous zinc-ion batteries. *Nano Energy* **2021**, *85*, 105969. [CrossRef]
36. Dai, Y.; Gan, Z.; Ruan, Y.; An, Q.; Mai, L. Research Progress of Aqueous Zinc Ion Batteries and Their Key Materials. *J. Chin. Ceram. Soc.* **2021**, *49*, 1323–1336.
37. Li, Y.; Chen, M.; Liu, B.; Zhang, Y.; Liang, X.; Xia, X. Heteroatom Doping: An Effective Way to Boost Sodium Ion Storage. *Adv. Energy Mater.* **2020**, *10*, 2000927. [CrossRef]
38. He, P.; Yan, M.; Zhang, G.; Sun, R.; Chen, L.; An, Q.; Mai, L. Layered VS_2 Nanosheet-Based Aqueous Zn Ion Battery Cathode. *Adv. Energy Mater.* **2017**, *7*, 1601920. [CrossRef]
39. Liu, Y.-Y.; Yuan, G.-Q.; Wang, X.-Y.; Liu, J.-P.; Zeng, Q.-Y.; Guo, X.-T.; Wang, H.; Liu, C.-S.; Pang, H. Tuning electronic structure of ultrathin V_6O_{13} nanobelts via nickel doping for aqueous zinc-ion battery cathodes. *Chem. Eng. J.* **2022**, *428*, 132538. [CrossRef]
40. Li, Q.; Wei, T.; Ma, K.; Yang, G.; Wang, C. Boosting the Cyclic Stability of Aqueous Zinc-Ion Battery Based on Al-Doped $V_{10}O_{24}{\cdot}12H_2O$ Cathode Materials. *Acs Appl. Mater. Interfaces* **2019**, *11*, 20888–20894. [CrossRef]
41. Lan, B.; Peng, Z.; Chen, L.; Tang, C.; Dong, S.; Chen, C.; Zhou, M.; Chen, C.; An, Q.; Luo, P. Metallic silver doped vanadium pentoxide cathode for aqueous rechargeable zinc ion batteries. *J. Alloy. Compd.* **2019**, *787*, 9–16. [CrossRef]
42. Wu, F.; Wang, Y.; Ruan, P.; Niu, X.; Zheng, D.; Xu, X.; Gao, X.; Cai, Y.; Liu, W.; Shi, W.; et al. Fe-doping enabled a stable vanadium oxide cathode with rapid Zn diffusion channel for aqueous zinc-ion batteries. *Mater. Today Energy* **2021**, *21*, 100842. [CrossRef]
43. Geng, H.; Cheng, M.; Wang, B.; Yang, Y.; Zhang, Y.; Li, C.C. Electronic Structure Regulation of Layered Vanadium Oxide via Interlayer Doping Strategy toward Superior High-Rate and Low-Temperature Zinc-Ion Batteries. *Adv. Funct. Mater.* **2020**, *30*, 1907684. [CrossRef]
44. Zhang, D.; Cao, J.; Yue, Y.; Pakornchote, T.; Bovornratanaraks, T.; Han, J.; Zhang, X.; Qin, J.; Huang, Y. Two Birds with One Stone: Boosting Zinc-Ion Insertion/Extraction Kinetics and Suppressing Vanadium Dissolution of V_2O_5 via La^{3+} Incorporation Enable Advanced Zinc-Ion Batteries. *Acs Appl. Mater. Interfaces* **2021**, *13*, 38416–38424. [CrossRef] [PubMed]
45. He, D.; Peng, Y.; Ding, Y.; Xu, X.; Huang, Y.; Li, Z.; Zhang, X.; Hu, L. Suppressing the skeleton decomposition in Ti-doped $NH_4V_4O_{10}$ for durable aqueous zinc ion battery. *J. Power Sources* **2021**, *484*, 229284. [CrossRef]
46. Guo, K.; Cheng, W.; Liu, H.; She, W.; Wan, Y.; Wang, H.; Li, H.; Li, Z.; Zhong, X.; Ouyang, J.; et al. Sn-Doped Hydrated V_2O_5 Cathode Material with Enhanced Rate and Cycling Properties for Zinc-Ion Batteries. *Crystals* **2022**, *12*, 1617. [CrossRef]

47. Li, M.; Mou, J.; Zhong, L.; Liu, T.; Xu, Y.; Pan, W.; Huang, J.; Wang, G.; Liu, M. Porous Ultrathin W-Doped VO_2 Nanosheets Enable Boosted Zn^{2+} (De)Intercalation Kinetics in VO2 for High-Performance Aqueous Zn-Ion Batteries. *Acs Sustain. Chem. Eng.* **2021**, *9*, 14193–14201. [CrossRef]
48. Li, Q.; Ye, X.; Jiang, Y.; Ang, E.H.; Liu, W.; Feng, Y.; Rui, X.; Yu, Y. Superior potassium and zinc storage in K-doped VO_2(B) spheres. *Mater. Chem. Front.* **2021**, *5*, 3132–3138. [CrossRef]
49. Lv, T.-T.; Luo, X.; Yuan, G.-Q.; Yang, S.-Y.; Pang, H. Layered VO_2@N-doped carbon composites for high-performance rechargeable aqueous zinc-ion batteries. *Chem. Eng. J.* **2022**, *428*, 131211. [CrossRef]
50. Wang, Z.; Zhang, M.; Ma, W.; Zhu, J.; Song, W. Application of Carbon Materials in Aqueous Zinc Ion Energy Storage Devices. *Small* **2021**, *17*, 2100219. [CrossRef]
51. Yu, P.F.; Zhou, J.X.; Zheng, M.T.; Li, M.R.; Hu, H.; Xiao, Y.; Liu, Y.L.; Liang, Y.R. Boosting zinc ion energy storage capability of inert MnO cathode by defect engineering. *J. Colloid Interface Sci.* **2021**, *594*, 540–549. [CrossRef]
52. Zhu, C.Y.; Fang, G.Z.; Liang, S.Q.; Chen, Z.X.; Wang, Z.Q.; Ma, J.Y.; Wang, H.; Tang, B.Y.; Zheng, X.S.; Zhou, J. Electrochemically induced cationic defect in MnO intercalation cathode for aqueous zinc-ion battery. *Energy Storage Mater.* **2020**, *24*, 394–401. [CrossRef]
53. Zhang, W.; Xiao, Y.; Zuo, C.; Tang, W.; Liu, G.; Wang, S.; Cai, W.; Dong, S.; Luo, P. Adjusting the Valence State of Vanadium in VO_2(B) by Extracting Oxygen Anions for High-Performance Aqueous Zinc-Ion Batteries. *Chemsuschem* **2021**, *14*, 971–978. [CrossRef] [PubMed]
54. Liao, M.; Wang, J.; Ye, L.; Sun, H.; Wen, Y.; Wang, C.; Sun, X.; Wang, B.; Peng, H. A Deep-Cycle Aqueous Zinc-Ion Battery Containing an Oxygen-Deficient Vanadium Oxide Cathode. *Angew. Chem.-Int. Ed.* **2020**, *59*, 2273–2278. [CrossRef] [PubMed]
55. He, T.; Weng, S.; Ye, Y.; Cheng, J.; Wang, X.; Wang, X.; Wang, B. Cation- deficient $Zn_{0.3}(NH_4)_{0.3}V_4O_{10}{\cdot}0.91H_2O$ for rechargeable aqueous zinc battery with superior low- temperature performance. *Energy Storage Mater.* **2021**, *38*, 389–396. [CrossRef]
56. Zhao, X.; Mao, L.; Cheng, Q.; Liao, F.; Yang, G.; Lu, X.; Chen, L. Interlayer Engineering of Preintercalated Layered Oxides as Cathode for Emerging Multivalent Metal-ion Batteries: Zinc and Beyond. *Energy Storage Mater.* **2021**, *38*, 397–437. [CrossRef]
57. Xu, Y.; Deng, X.; Li, Q.; Zhang, G.; Xiong, F.; Tan, S.; Wei, Q.; Lu, J.; Li, J.; An, Q.; et al. Vanadium Oxide Pillared by Interlayer Mg^{2+} Ions and Water as Ultralong-Life Cathodes for Magnesium-Ion Batteries. *Chem* **2019**, *5*, 1194–1209. [CrossRef]
58. Shi, W.; Yin, B.; Yang, Y.; Sullivan, M.B.; Wang, J.; Zhang, Y.-W.; Yu, Z.G.; Lee, W.S.V.; Xue, J. Unravelling V6O13 Diffusion Pathways via CO_2 Modification for High-Performance Zinc Ion Battery Cathode. *Acs Nano* **2021**, *15*, 1273–1281. [CrossRef] [PubMed]
59. Li, W.; Han, C.; Gu, Q.; Chou, S.-L.; Wang, J.-Z.; Liu, H.-K.; Dou, S.-X. Electron Delocalization and Dissolution-Restraint in Vanadium Oxide Superlattices to Boost Electrochemical Performance of Aqueous Zinc-Ion Batteries. *Adv. Energy Mater.* **2020**, *10*, 2001852. [CrossRef]
60. Chen, S.; Li, K.; Hui, K.S.; Zhang, J. Regulation of Lamellar Structure of Vanadium Oxide via Polyaniline Intercalation for High-Performance Aqueous Zinc-Ion Battery. *Adv. Funct. Mater.* **2020**, *30*, 2003890. [CrossRef]
61. Li, R.; Xing, F.; Li, T.; Zhang, H.; Yan, J.; Zheng, Q.; Li, X. Intercalated polyaniline in V_2O_5 as a unique vanadium oxide bronze cathode for highly stable aqueous zinc ion battery. *Energy Storage Mater.* **2021**, *38*, 590–598. [CrossRef]
62. Bin, D.; Huo, W.; Yuan, Y.; Huang, J.; Liu, Y.; Zhang, Y.; Dong, F.; Wang, Y.; Xia, Y. Organic-Inorganic-Induced Polymer Intercalation into Layered Composites for Aqueous Zinc-Ion Battery. *Chem* **2020**, *6*, 968–984. [CrossRef]
63. Feng, Z.; Sun, J.; Liu, Y.; Jiang, H.; Cui, M.; Hu, T.; Meng, C.; Zhang, Y. Engineering Interlayer Space of Vanadium Oxide by Pyridinesulfonic Acid-Assisted Intercalation of Polypyrrole Enables Enhanced Aqueous Zinc-Ion Storage. *Acs Appl. Mater. Interfaces* **2021**, *13*, 61154–61165. [CrossRef] [PubMed]
64. Liu, Z.; Sun, H.; Qin, L.; Cao, X.; Zhou, J.; Pan, A.; Fang, G.; Liang, S. Interlayer Doping in Layered Vanadium Oxides for Low-cost Energy Storage: Sodium-ion Batteries and Aqueous Zinc-ion Batteries. *Chemnanomat* **2020**, *6*, 1553–1566. [CrossRef]
65. Yang, Y.; Tang, Y.; Liang, S.; Wu, Z.; Fang, G.; Cao, X.; Wang, C.; Lin, T.; Pan, A.; Zhou, J. Transition metal ion-preintercalated V_2O_5 as high-performance aqueous zinc-ion battery cathode with broad temperature adaptability. *Nano Energy* **2019**, *61*, 617–625. [CrossRef]
66. Wan, F.; Niu, Z.Q. Design Strategies for Vanadium-based Aqueous Zinc-Ion Batteries. *Angew. Chem.-Int. Ed.* **2019**, *58*, 16358–16367. [CrossRef] [PubMed]
67. Tamilselvan, M.; Sreekanth, T.V.M.; Yoo, K.; Kim, J. Wide interlayer spacing ammonium vanadate $(NH_4)_{0.37}V_2O_5{\cdot}0.15H_2O$ cathode for rechargeable aqueous zinc-ion batteries. *J. Ind. Eng. Chem.* **2021**, *93*, 176–185. [CrossRef]
68. Wei, T.; Li, Q.; Yang, G.; Wang, C. Highly reversible and long-life cycling aqueous zinc-ion battery based on ultrathin $(NH_4)_2V_{10}O_{25}{\cdot}8H_2O$ nanobelts. *J. Mater. Chem. A* **2018**, *6*, 20402–20410. [CrossRef]
69. Huang, M.; Wang, X.; Liu, X.; Mai, L. Fast Ionic Storage in Aqueous Rechargeable Batteries: From Fundamentals to Applications. *Adv. Mater.* **2022**, *34*, 2105611. [CrossRef] [PubMed]
70. Zhang, Y.; Chen, A.; Sun, J. Promise and challenge of vanadium-based cathodes for aqueous zinc-ion batteries. *J. Energy Chem.* **2021**, *54*, 655–667. [CrossRef]
71. Yin, Z.G.; Zheng, Q.D. Controlled Synthesis and Energy Applications of One-Dimensional Conducting Polymer Nanostructures: An Overview. *Adv. Energy Mater.* **2012**, *2*, 179–218. [CrossRef]
72. Yang, Y.; Yu, G.H.; Cha, J.J.; Wu, H.; Vosgueritchian, M.; Yao, Y.; Bao, Z.A.; Cui, Y. Improving the Performance of Lithium-Sulfur Batteries by Conductive Polymer Coating. *Acs Nano* **2011**, *5*, 9187–9193. [CrossRef] [PubMed]

73. Zhang, H.; Yao, Z.; Lan, D.; Liu, Y.; Ma, L.; Cui, J. N-doped carbon/V_2O_3 microfibers as high-rate and ultralong-life cathode for rechargeable aqueous zinc-ion batteries. *J. Alloy. Compd.* **2021**, *861*, 158560. [CrossRef]
74. Pang, Q.; Sun, C.; Yu, Y.; Zhao, K.; Zhang, Z.; Voyles, P.M.; Chen, G.; Wei, Y.; Wang, X. $H_2V_3O_8$ Nanowire/Graphene Electrodes for Aqueous Rechargeable Zinc Ion Batteries with High Rate Capability and Large Capacity. *Adv. Energy Mater.* **2018**, *8*, 1800144. [CrossRef]
75. Zhang, Z.; Xi, B.; Wang, X.; Ma, X.; Chen, W.; Feng, J.; Xiong, S. Oxygen Defects Engineering of $VO_2 \cdot xH_2O$ Nanosheets via In Situ Polypyrrole Polymerization for Efficient Aqueous Zinc Ion Storage. *Adv. Funct. Mater.* **2021**, *31*, 2103070. [CrossRef]
76. Volkov, F.S.; Tolstopjatova, E.G.; Eliseeva, S.N.; Kamenskii, M.A.; Vypritskaia, A.I.; Volkov, A.I.; Kondratiev, V.V. Vanadium(V) oxide coated by poly(3,4-ethylenedioxythiophene) as cathode for aqueous zinc-ion batteries with improved electrochemical performance. *Mater. Lett.* **2022**, *308*, 131210. [CrossRef]
77. Bard, A.J. Photoelectrochemistry And Heterogeneous Photocatalysis at Semiconductors. *J. Photochem.* **1979**, *10*, 59–75. [CrossRef]
78. Chen, J.; Xiao, B.; Hu, C.; Chen, H.; Huang, J.; Yan, D.; Peng, S. Construction Strategy of VO_2@V_2C 1D/2D Heterostructure and Improvement of Zinc-Ion Diffusion Ability in VO_2(B). *Acs Appl. Mater. Interfaces* **2022**, *14*, 28760–28768. [CrossRef]
79. Zhao, F.; Gong, S.; Xu, H.; Li, M.; Li, L.; Qi, J.; Wang, H.; Wang, Z.; Hu, Y.; Fan, X.; et al. In situ constructing amorphous V_2O_5@$Ti_3C_2T_x$ heterostructure for high-performance aqueous zinc-ion batteries. *J. Power Sources* **2022**, *544*, 231883. [CrossRef]
80. Zhu, K.; Wu, T.; Huang, K. A high-voltage activated high-erformance cathode for aqueous Zn-ion batteries. *Energy Storage Mater.* **2021**, *38*, 473–481. [CrossRef]
81. Wu, T.-H.; Su, J.-H. Controlling crystal structures of vanadium oxides via pH regulation and decoupling crystallographic perspective on zinc storage behaviors. *Acta Mater.* **2023**, *245*, 118663. [CrossRef]
82. Lu, H.; Li, X. Inhibition of Zinc Dendrite Growth in Zinc-Based Batteries. *ChemSusChem* **2018**, *11*, 3996–4006. [CrossRef] [PubMed]
83. Turney, D.E.; Gallaway, J.W.; Yadav, G.G.; Ramirez, R.; Nyce, M.; Banerjee, S.; Chen-Wiegart, Y.-C.K.; D'Ambrose, M.J.; Huang, J.; Wei, X. Rechargeable Zinc Alkaline Anodes for Long-Cycle Energy Storage. *Chem. Mater.* **2017**, *29*, 4819–4832. [CrossRef]
84. Zhao, K.; Wang, C.; Yu, Y.; Yan, M.; Wei, Q.; He, P.; Dong, Y.; Zhang, Z.; Wang, X.; Mai, L. Ultrathin Surface Coating Enables Stabilized Zinc Metal Anode. *Adv. Mater. Interfaces* **2018**, *5*, 1800848. [CrossRef]
85. Chen, P.; Yuan, X.; Xia, Y.; Zhang, Y.; Fu, L.; Liu, L.; Yu, N.; Huang, Q.; Wang, B.; Hu, X.; et al. An Artificial Polyacrylonitrile Coating Layer Confining Zinc Dendrite Growth for Highly Reversible Aqueous Zinc-Based Batteries. *Adv. Sci.* **2021**, *8*, 2100309. [CrossRef]
86. Verma, V.; Kumar, S.; Manalastas, W., Jr.; Srinivasan, M. Undesired Reactions in Aqueous Rechargeable Zinc Ion Batteries. *Acs Energy Lett.* **2021**, *6*, 1773–1785. [CrossRef]
87. Cao, H.; Huang, X.; Li, Y.; Liu, Y.; Zheng, Q.; Huo, Y.; Zhao, R.; Zhao, J.; Lin, D. Regulating the solventized structure to achieve highly reversible zinc plating/stripping for dendrite-free Zn anode by sulfolane additive. *Chem. Eng. J.* **2023**, *455*, 140538. [CrossRef]
88. Ni, Q.; Kim, B.; Wu, C.; Kang, K. Non-Electrode Components for Rechargeable Aqueous Zinc Batteries: Electrolytes, Solid-Electrolyte-Interphase, Current Collectors, Binders, and Separators. *Adv. Mater.* **2022**, *34*, 2108206. [CrossRef]
89. Li, Z.; Ye, L.; Zhou, G.; Xu, W.; Zhao, K.; Zhang, X.; Hong, S.; Ma, T.; Li, M.-C.; Liu, C.; et al. A water-gating and zinc-sieving lignocellulose nanofiber separator for dendrite-free rechargeable aqueous zinc ion battery. *Chem. Eng. J.* **2023**, *457*, 141160. [CrossRef]
90. Guo, C.; Yi, S.; Si, R.; Xi, B.; An, X.; Liu, J.; Li, J.; Xiong, S. Advances on Defect Engineering of Vanadium-Based Compounds for High-Energy Aqueous Zinc-Ion Batteries. *Adv. Energy Mater.* **2022**, *12*, 2202039. [CrossRef]

Disclaimer/Publisher's Note: The statements, opinions and data contained in all publications are solely those of the individual author(s) and contributor(s) and not of MDPI and/or the editor(s). MDPI and/or the editor(s) disclaim responsibility for any injury to people or property resulting from any ideas, methods, instructions or products referred to in the content.